Autoionization rates of core-excited magnesium Rydberg atoms in electric fields using the core fluorescence as a reference

D. Wehrli, M. Génévriez, and F. Merkt
Laboratory of Physical Chemistry, ETH Zürich, CH-8093 Zürich, Switzerland

(Received 18 April 2019; published 24 July 2019)

$[M^{+*}]nl$ core-excited Rydberg states of the alkaline-earth-metal atoms can decay by electronic autoionization ($[M^{+*}]nl \rightarrow M^+ + \varepsilon l'$) or by fluorescence of the core ($[M^{+*}]nl \rightarrow [M^+]nl + h\nu$). The two processes can be detected separately by monitoring the prompt M^+ autoionization yield and the delayed pulsed-field-ionization yield of the $[M^+]nl$ Rydberg states. Whereas the former process strongly depends on the principal (n) and orbital angular-momentum (l) quantum numbers, the latter is independent of n and l because it is essentially a property of the ion core. We present an experimental study of the competition between autoionization and core fluorescence in $[Ne]3p_{3/2}nl$ core-excited Rydberg states of Mg atoms and of its dependence on n and weak electric fields. We analyze the experimental results using a kinetic model, from which we extract the electronic-autoionization rates by using the Mg^+ $3p_{3/2}$–$3s_{1/2}$ core fluorescence ($\tau_{fl} = 3.8$ ns) as an internal clock. The autoionization rate of the $3p_{3/2}nd_{3/2}$ ($J = 3$) and of the fully Stark-mixed $3p_{3/2}nk$ ($m = 0, \pm 2$) series are $[1.9 \times 10^{16}/n^{*3}]$ s^{-1} and $[8(3) \times 10^{15}/n^4]$ s^{-1}, which would translate for the lowest Rydberg states ($3d$ with $n^* = 2.62$) to autoionization rates of $\sim 10^{15}$ and $\sim 10^{14}$ s^{-1}, respectively, as fast as Auger decay processes.

DOI: 10.1103/PhysRevA.100.012515

I. INTRODUCTION

Doubly excited states of atoms and molecules are states in which two electrons have been promoted to orbitals not occupied in the ground electronic state. The high energies typically required for the excitation of two electrons and their correlated motion give rise to complex dynamics, with multiple competing radiative and nonradiative channels [1]. Alkaline-earth metals and Yb are ideal systems to study such states because they have two valence electrons.

Core-excited Rydberg states are an important class of doubly excited states, in which one of the two electrons is in a Rydberg state of low principal quantum number n (or a valence state in molecules) and the other one is in a high-n Rydberg state, which can be regarded as orbiting around an electronically excited ion core. Such states are reminiscent of two-planet solar systems, in which one planet would be Venus-like, the other Pluto-like, although often the term planetary atom is used for atoms with excited electrons in nonpenetrating high-l orbits, see, e.g., Refs. [2–8]. Core-excited Rydberg states, denoted $[M^{+*}]nl$ below, play an important role in plasmas by resonantly enhancing electron-ion radiative-association reactions through the process of dielectronic recombination [9–24],

$$M^+ + e^- \rightleftarrows [M^{+*}]nl \rightarrow [M^+]nl + h\nu, \qquad (1)$$

illustrated on the right-hand side of Fig. 1 with the example of Mg. They can also be accessed by exciting the ion core of a Rydberg atom and be observed as autoionizing resonances in photoionization spectra (see Ref. [8] for a recent example)

$$[M^+]nl + h\nu \rightleftarrows [M^{+*}]nl \rightarrow M^+ + e^-. \qquad (2)$$

In Eqs. (1) and (2), M^+ represents the electronic ground state of the ion ($[Ne]3s$ in the case of Mg^+) and $[M^+]nl$ a high Rydberg state.

In atoms $[M^{+*}]nl$ can decay by autoionization or by core fluorescence (Mg $3p_{3/2}nl$–$3s_{1/2}nl$ in the present case) and the branching ratio between these two competing processes is determined by their rates. The autoionization rate reflects the probability of finding the Rydberg electron in the core region and scales with the effective principal quantum number n^* as n^{*-3}. The rate also rapidly decreases with increasing angular-momentum quantum number l. At high n and/or l values the Rydberg electron hardly interacts with the ion core so that the core fluorescence rate is essentially independent of n and l. Consequently, at sufficiently high n and/or l values the core fluorescence inevitably becomes the dominant decay process in core-excited Rydberg states. In this regime, the atom exists in a planetary-like doubly excited state until the core fluoresces.

The competition between autoionization and core fluorescence is strongly influenced by electric fields. At high n values, even weak electric fields can induce strong l mixing in Rydberg states [25–27]. l-mixed Rydberg states autoionize much more slowly than low-l states because of the non-core-penetrating character of high-l states [26]. At the same time, l mixing enhances dielectronic recombination [11].

Core-excited Rydberg states offer attractive properties in experiments for quantum optics and quantum-information processing [28–30]. The long-range potential resulting from the large dipole moment associated with the Rydberg electron can be exploited to study Rydberg-Rydberg atom interactions and many-body dynamics under conditions where the core transitions involving the second valence electron are used to manipulate the motion of the atoms and probe them [28]. Core-excited Rydberg states are easily imaged by collecting either the core fluorescence or the ions resulting from autoionization [31–33]. These applications rely on the decoupling of the Rydberg electron from the ion core, which forms the basis of the isolated-core excitation (ICE) method [34–36]. The

 ©2019 American Physical Society

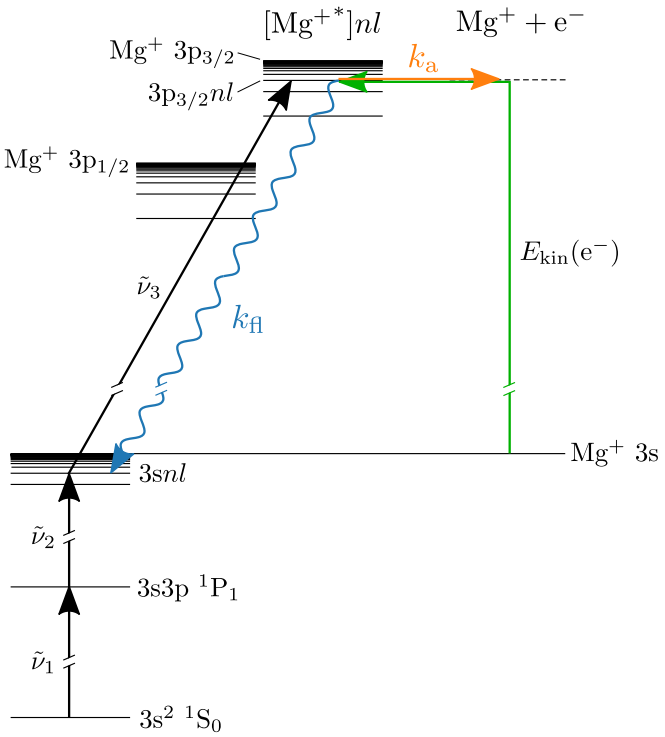

FIG. 1. Multiphoton excitation scheme used to access the $3p_{3/2}nl$ core-excited Rydberg states of Mg. The decay of the core-excited Rydberg states by core fluorescence and autoionization is designated by arrows labeled k_{fl} and k_a, respectively. The green left-facing horizontal arrow indicates the first step of the dielectronic recombination. The transition labeled $\tilde{\nu}_3$ corresponds to the isolated-core excitation.

decoupling can be achieved in three ways: (i) by increasing the principal quantum number n, as illustrated in the recent experiments of Fields *et al.* [8], (ii) by increasing the orbital angular momentum of the Rydberg electron, as demonstrated, e.g., by Pruvost *et al.* [37] and more recently by Lehec [38], and (iii) by using the Stark effect to enhance the nonpenetrating character of the Rydberg electron through l mixing [8]. In terms of the competition between core fluorescence and autoionization discussed above, perfect ICE conditions imply a suppression of autoionization.

We present an experimental study of the core-fluorescence and autoionization dynamics in core-excited Rydberg states of Mg. We exploit the competitive nature of the fluorescence and autoionization kinetics to extract reliable rates for these processes in core-excited Rydberg states of Mg in dependence of n and in the regime where electric fields induce full l mixing. Emphasis is placed on the characterization of the conditions (n, electric fields) required for the complete suppression of autoionization and for the Rydberg electron to reach a pure spectator role in the dynamics of the doubly excited states.

II. EXPERIMENTAL SETUP

The experimental setup has been described in detail in Ref. [39] and includes a laser-ablation source of Mg atoms, three Nd:YAG-pumped dye lasers to excite the atoms to core-excited Rydberg states, and a detection system for the Mg^+ ions produced following photoexcitation. The Mg atoms were generated by laser ablation of a magnesium rod using a frequency-doubled Q-switched Nd:YAG laser and were subsequently entrained in a pulsed supersonic beam of N_2. The beam passed through a 4-mm-diameter skimmer located 8 cm downstream from the ablation spot and entered the photoexcitation chamber. In this chamber, the supersonic beam intersected the laser beams used for photoexcitation at right angles within a cylindrical electrode stack used to apply pulsed or static electric fields.

The magnesium atoms were excited to $3p_{3/2}nl$ core-excited Rydberg states using the three-photon excitation scheme depicted in Fig. 1. Here and in the following, we use nl to indicate both nd Rydberg states and nk Stark states. The outputs of the dye lasers were frequency-doubled using beta-barium-borate (BBO) crystals and their fundamental wave numbers were calibrated using a commercial wave meter with a specified accuracy of 0.02 cm^{-1}. The polarization of the frequency-doubled radiation of all lasers was perpendicular to the electric fields applied across the electrode stack. The wave number $\tilde{\nu}_1$ of the first laser was set to the position of the $3s^2\ ^1S_0$–$3s3p\ ^1P_1$ transition at $\tilde{\nu}_1 = 35051.26\ cm^{-1}$. The $3s_{1/2}nl$ Rydberg states were accessed by tuning the wave number $\tilde{\nu}_2$ of the second laser in the range from $\tilde{\nu}_2 = 26590\ cm^{-1}$ to $\tilde{\nu}_2 = 26620\ cm^{-1}$. Both lasers had a bandwidth of ∼0.15 cm^{-1}, a pulse length of ∼5 ns, and a beam diameter of ∼1 mm at the photoexcitation spot. To prevent (1 + 1) resonance-enhanced two-photon ionization by the first laser, its pulse energy was reduced to well below 1 μJ by deoptimizing the laser polarization before the BBO crystal with a half-wave plate and by rotating the BBO crystal away from the phase-matching angle. The ∼1 mJ pulse energy of the second laser was sufficient to saturate the excitation to the Rydberg states. The third laser (bandwidth ∼0.08 cm^{-1}, pulse length 4.4 ns, beam diameter ∼1 mm) induced the $3s_{1/2}$–$3p_{3/2}$ transition of the Mg^+ ion core at $\tilde{\nu}_3 = 35760.9\ cm^{-1}$, resulting in the formation of $3p_{3/2}nl$ core-excited Rydberg states. The energy of the third laser was set to ∼0.5 mJ per pulse to saturate the transition, which facilitates the quantitative analysis of the measurements, see Sec. IV. To prevent photoionization of the $3s3p\ ^1P_1$ intermediate state (radiative lifetime $\tau = 2.0$ ns [40]) by the third laser, this laser was delayed by ∼10 ns with respect to the first two lasers.

Approximately 2 μs after the laser excitation, an electric-field pulse (referred to as pre-pulse in the following) in the range between −0.5 and −1 V/cm was applied for ∼2 μs to spatially separate ions produced either by rapid autoionization or direct ionization (called prompt ions hereafter) from ions generated by pulsed-field ionization (PFI) of long-lived Rydberg states (called delayed ions) using a second, larger electric-field pulse of +70 V/cm, referred to as the extraction pulse. The two sets of ions were accelerated by the extraction pulse through a linear time-of-flight (TOF) tube toward a microchannel-plate detector. The spatial separation of prompt and delayed ions by the pre-pulse allowed us to distinguish between the two types of ions through their times of flight. The magnitude and delay of the two pulses were carefully chosen so as to also separate the three natural isotopes of magnesium.

In the experiment, dc potentials can also be applied across the electrode stack, either to compensate stray electric fields or to study how l mixing induced by the Stark effect influences the decay dynamics of the core-excited Rydberg states. We applied dc electric fields in the range between −862 and +86 mV/cm for the different measurements.

Each measurement consisted of scanning the wave number of the second laser, keeping the wave numbers of the other two lasers constant. While scanning, TOF spectra were recorded and averaged over 50 experimental cycles. The prompt and delayed $^{24}Mg^+$ ion signals were determined by fitting the sum of two Gaussian functions to the TOF distribution. This procedure had the advantage that reliable values for the relative signal strengths could be extracted even when the separation of the prompt and delayed ion signals by the pre-pulse was incomplete.

The prompt (I_{pr}) and delayed (I_{del}) signals obtained in a typical measurement are displayed in Figs. 2(a) and 2(b). Three processes contribute to the prompt ion signal: (i) rapid autoionization of the $3p_{3/2}nl$ core-excited Rydberg states, (ii) PFI of long-lived $3s_{1/2}nl$ Rydberg states by the pre-pulse, and (iii) direct ionization in the continuum above the Mg^+ ($3s\ ^2S_{1/2}$) ionization threshold, the position of which typically depends on the value of the applied dc field. The spectral regions in which each of these three processes dominates are labeled (i)–(iii) in Fig. 2. The delayed ion signal originates from the PFI of long-lived $3s_{1/2}nl$ Rybderg states regardless of whether core excitation by the third laser has taken place or not. Our experiments never yield a PFI signal for the $3p_{3/2}nl$ core-excited Rydberg states because both the pre-pulse and the extraction pulse are applied after these states have already decayed either by autoionization or core fluorescence, whichever is faster, and the core-fluorescence lifetime is only $\tau_{fl} = 3.8$ ns [40].

The magnitude of the prompt signal rises by a factor of about 2 between the lower part of region (i) and region (iii). This behavior reflects the saturation of the $3s3p\ ^1P_1$–$3s_{1/2}nl$ transition by the second laser. In the bound part of the Rydberg series, the population equilibrates between the $3s3p\ ^1P_1$ and the $3s_{1/2}nl$ Rydberg states. In region (iii) the second laser drains the entire population into the ionization continuum. The intensity distributions of the prompt and delayed ion signals are complementary and the dip in the prompt signal between region (i) and (iii) is exactly compensated for by the rise of the delayed ion signal.

From the ion signals displayed in Figs. 2(a) and 2(b), we extract the branching ratios

$$N_{pr} = \frac{I_{pr}}{I_{pr} + I_{del}} \tag{3}$$

and

$$N_{del} = \frac{I_{del}}{I_{pr} + I_{del}} \tag{4}$$

presented in Fig. 2(c). In region (i) the branching ratios N_{pr} and N_{del} correspond to the autoionization and core-fluorescence yields, respectively. Because the prompt and delayed ion signals are both subject to the same shot-to-shot fluctuations of the lasers and magnesium-ablation source, the branching ratios are nearly noise free and fully reproducible,

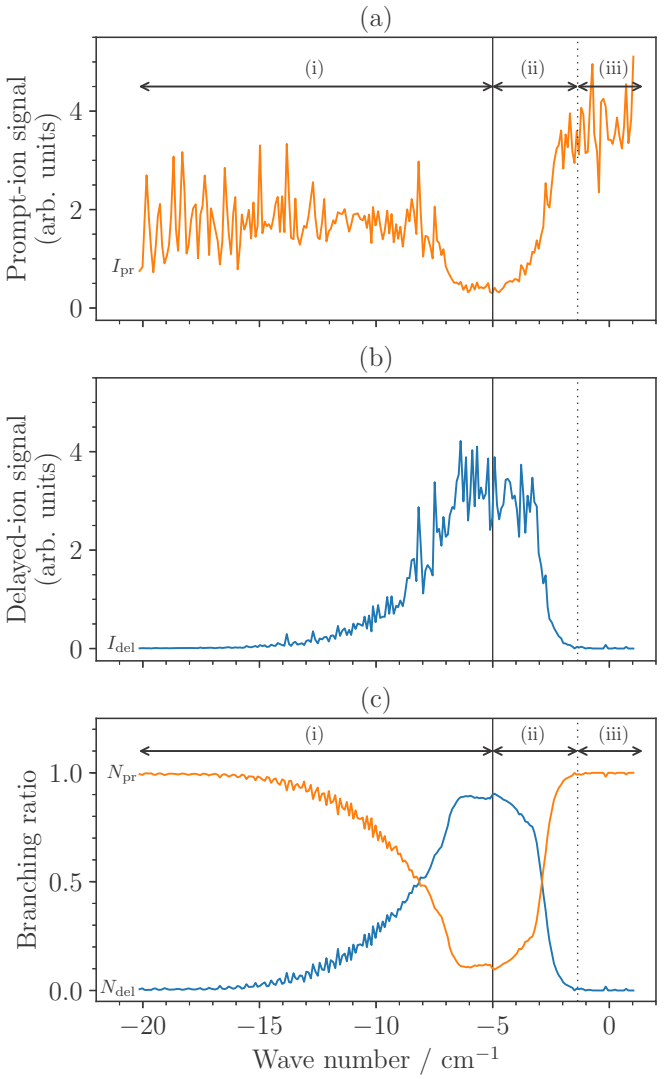

FIG. 2. Prompt (a) and delayed (b) Mg^+ ion signal obtained for a dc field of −49 mV/cm when scanning the second laser in the vicinity of the $Mg^+(3s\ ^2S_{1/2})$ ionization threshold. The regions labeled (i)–(iii) and separated by vertical lines are the regions where the dominant mechanisms for the production of prompt ions are (i) the autoionization of the $3p_{3/2}nl$ core-excited Rydberg states, (ii) the PFI of $3s_{1/2}nl$ Rydberg states, and (iii) direct ionization into the $3s\ ^2S_{1/2}$ ionization continuum (see text for details). (c) Branching ratios for the production of the prompt (N_{pr}) and delayed (N_{del}) ions. The wave-number scale is given relative to the field-free ionization threshold.

an advantage we exploit in the quantitative analysis of the data, see Sec. IV. Another advantage is that the factor-of-2 increase in the total ionization signal mentioned above cancels out.

At wave numbers above the onset of the field-ionization signal induced by the pre-pulse (see solid vertical line in Fig. 2), the pre-pulse collects both the autoionization and the PFI signal from long-lived $3s_{1/2}nl$ Rydberg states, which prevents the distinction between autoionization and core fluorescence in region (ii). This region thus cannot be used in our analysis. Region (iii) is also irrelevant because in

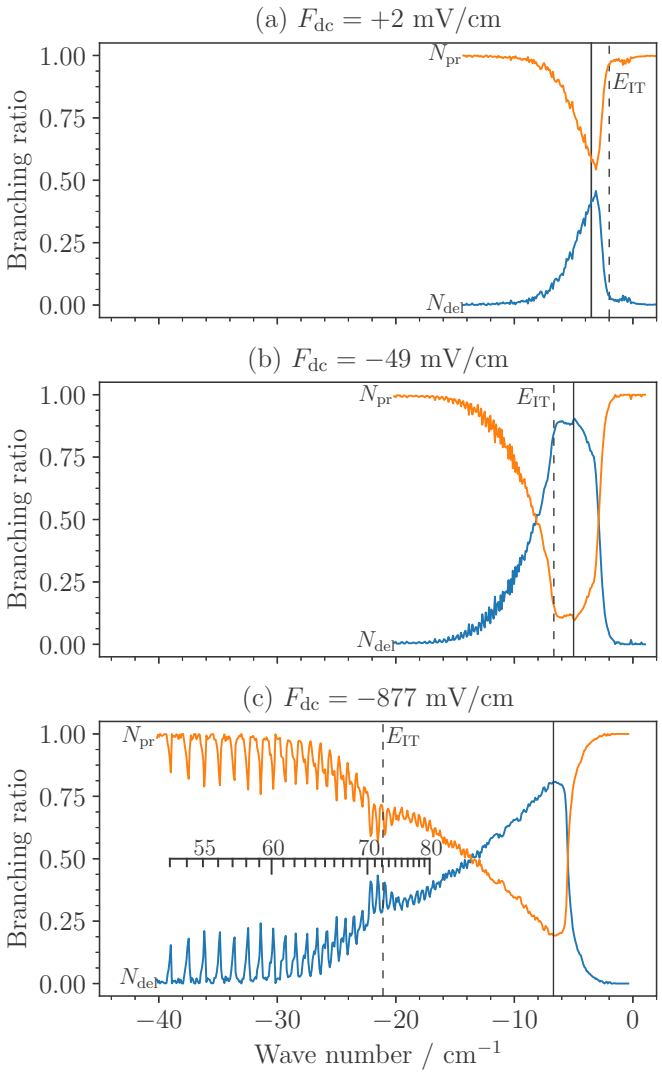

FIG. 3. Branching ratios recorded at different dc field strengths F_{dc} of 2 mV/cm (a), −49 mV/cm (b), and −877 mV/cm (c). The values of F_{dc} are corrected by the electric stray field present in the photoexcitation region. The signal originating from autoionization is denoted N_{pr} and the Rydberg signal is denoted N_{del}. The solid vertical lines mark the onset of field ionization by the pre-pulse. The dashed vertical lines indicate the Inglis-Teller limit E_{IT} where adjacent Stark manifolds start overlapping. The series of peaks labeled in (c) corresponds to a Rydberg series with zero quantum defect, i.e., to high-l Rydberg states. The wave-number scale is given relative to the field-free ionization threshold.

this region the ions are generated by the first two lasers exclusively.

III. EXPERIMENTAL RESULTS AND QUALITATIVE BEHAVIOR

Figures 3(a)–3(c) present spectra of high Mg Rydberg states obtained by scanning the second laser in the presence of three different dc fields F_{dc} of +2, −49, and −877 mV/cm, respectively, under otherwise similar experimental conditions. The differences in these spectra thus originate from the Stark effect. In each spectrum, the zero of the wave-number scale corresponds to the field-free ionization threshold of Mg. The laser bandwidth is too large for individual Rydberg states to be resolved beyond $n \approx 80$, i.e., within 17 cm^{-1} of the field-free ionization threshold. In all three spectra, the prompt ion signal dominates at low energies. The delayed ion signal grows as the ionization threshold is approached, but returns to zero at the onset of the field ionization by the pre-pulse, which is marked by the full vertical lines in Fig. 3.

The dashed vertical lines indicate the positions of the Inglis-Teller limits corresponding to the values of the dc electric fields present at the time of photoexcitation. The Inglis-Teller limit corresponds to the n value at which, for a given dc electric field, adjacent Stark manifolds start overlapping spectrally and l mixing is extensive. It is given, in atomic units, by [26]

$$F = \frac{1}{3n^5}. \tag{5}$$

At lower fields, some degree of l mixing already exists, which increases with increasing field strength. The branching ratios and their evolution with increasing dc field enable one to conclude that (i) l mixing between the optically accessible low-l Rydberg states (nd in the present case) and nonpenetrating high-l states is a necessary condition for the observation of a delayed signal in our experiments, and (ii) in the absence of l mixing, the nd Rydberg states autoionize on a timescale shorter than the core-fluorescence lifetime ($\tau_{fl} = 3.8$ ns [40]), even at n values as high as 200. l mixing by electric fields reduces the short-lived low-l character of the eigenstates and increases their lifetimes by a factor of $\sim n$ [25].

The strong dependence of the onset of the delayed ion signal on the value of the dc electric field was actually used to determine the stray electric field present in the photoexcitation region. A stray field of −15 mV/cm was determined by varying the strength of the electric field applied along the axis of the electrode stack and by minimizing the delayed ion signal. The values of F_{dc} given in Fig. 3 are already corrected for the stray field. Stray fields perpendicular to the applied dc field were significantly smaller because of the cylindrical symmetry of the electrode stack.

A series of well-resolved lines is observed in Fig. 3(c). Their positions correspond exactly to high-l Rydberg series of zero quantum defect. These series gain intensity through Stark mixing with the nd series, but have long lifetimes because of their dominant high-l character. In all spectra, including several spectra recorded at other F_{dc} values than those shown in Fig. 3, we observe a local maximum of the delayed ion signal close to the Inglis-Teller limit, e.g., at n values in the range 70–72 in Fig. 3(c). Judging from the experimental data, the Inglis-Teller limit thus seems to represent the ideal compromise between efficient photoexcitation, which requires sufficient d character, and long lifetimes, which requires a large nonpenetrating high-l character.

IV. DETERMINATION OF AUTOIONIZATION RATES

To extract autoionization rates from the branching ratios we use a kinetic model that treats the photoexcitation by the third laser separately from the subsequent laser-field-free evolution. In the first period ($0 < t < \tau$) we assume that the branching ratio corresponding to the prompt ion signal N_{pr}

builds up according to

$$N_{\rm pr}(\tau) = 1 - \exp(-k_{\rm a}\tau/2), \tag{6}$$

where τ is the effective interaction time with the third laser and $k_{\rm a}$ is the autoionization rate of the $3p_{3/2}nl$ core-excited Rydberg state. The factor $1/2$ in the exponent comes from the fact that on average half of the Rydberg-atom population is in the $3p_{3/2}nl$ state because of saturation.

Saturation also implies that at the beginning of the laser-field-free evolution ($t = \tau$) the populations $N_{\rm del}$ and N_{3p} of the singly excited $3s_{1/2}nl$ and autoionizing $3p_{3/2}nl$ Rydberg states, respectively, are equal,

$$N_{\rm del}(\tau) = N_{3p}(\tau) = \tfrac{1}{2}\exp(-k_{\rm a}\tau/2). \tag{7}$$

In the laser-field-free regime ($t > \tau$), the kinetics is governed by the decay of the core-excited Rydberg states by autoionization with rate $k_{\rm a}$ and fluorescence with rate $k_{\rm fl}$,

$$\frac{dN_{\rm del}}{dt} = k_{\rm fl}N_{3p}, \tag{8a}$$

$$\frac{dN_{3p}}{dt} = -(k_{\rm fl} + k_{\rm a})N_{3p}, \tag{8b}$$

$$\frac{dN_{\rm pr}}{dt} = k_{\rm a}N_{3p}. \tag{8c}$$

Using Eqs. (6) and (7) as initial conditions and assuming that detection takes place at $t \gg \tau$ yields the branching ratios

$$N_{\rm pr} = 1 - \exp(-k_{\rm a}\tau/2)\left[1 - \frac{1}{2}\frac{k_{\rm a}}{k_{\rm fl} + k_{\rm a}}\right] \tag{9}$$

and

$$N_{\rm del} = \frac{1}{2}\exp(-k_{\rm a}\tau/2)\left[1 + \frac{k_{\rm fl}}{k_{\rm fl} + k_{\rm a}}\right], \tag{10}$$

for which experimental results are displayed in Fig. 3. Equations (9) and (10) can be used to determine the autoionization rate $k_{\rm a}$ from the experimental data at any excitation wave number and external field $F_{\rm dc}$ provided that the remaining parameters τ and $k_{\rm fl}$ are known. For $k_{\rm fl}$ we use the fluorescence rate $k_{\rm fl} = 2.6 \times 10^8$ s^{-1} of the Mg^+ $3p_{3/2}$–Mg^+ $3s_{3/2}$ transition [40] and for τ we choose $\tau = 8.8$ ns, which is twice the pulse length (FWHM) of the third laser to account for the level of saturation characteristic of our measurement.

Figure 4(a) depicts the experimental data already presented in Fig. 3(c) but after conversion of the wave-number scale into an effective-principal-quantum-number scale. The n-dependent autoionization rates $k_{\rm a}(n)$ shown in Fig. 4(b) are extracted from the branching ratios by direct inversion of Eqs. (9) and (10). The core fluorescence thus represents an internal clock for the determination of $k_{\rm a}$. The full circles in Fig. 4(b) correspond to the range of n values ($n > 90$) where the dc electric field ($F_{\rm dc} = -877$ mV/cm) induces strong l mixing. In this range, the branching ratios are not affected by small changes of the dc-field strength, which indicates that the regime of full l mixing is reached. Consequently, the autoionization rate $k_{\rm a}$ can be expressed as [25,26]

$$k_{\rm a}(n) = \gamma^{\rm Stark}/n^4, \tag{11}$$

where $\gamma^{\rm Stark}$ is the n-independent scaled autoionization rate for the limiting case of complete l mixing. A field of

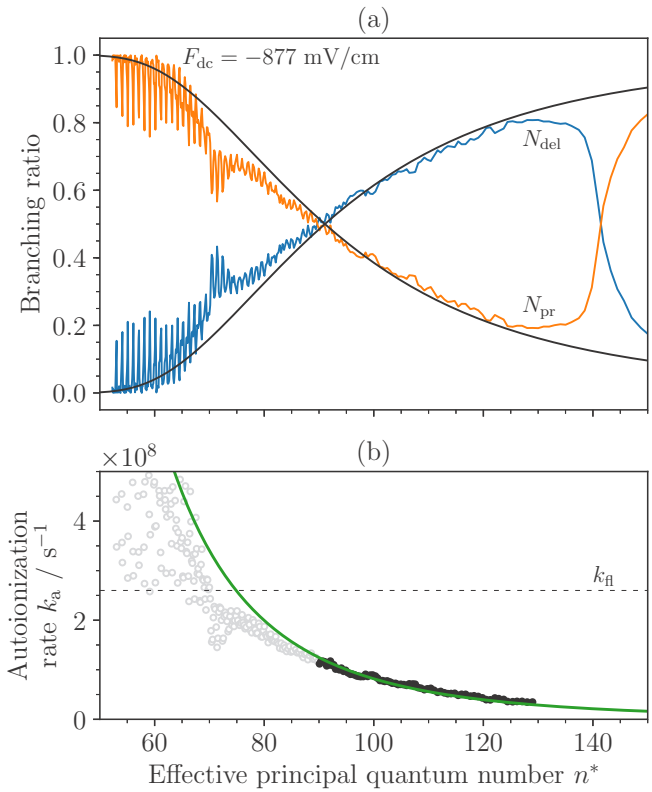

FIG. 4. (a) Branching ratios, measured at a dc field $F_{\rm dc} = -877$ mV/cm, for the decay of core-excited Rydberg states of Mg by autoionization ($N_{\rm pr}$) and core fluorescence ($N_{\rm del}$) displayed as a function of the effective quantum number n^*. (b) Autoionization rates $k_{\rm a}(n)$ determined using Eqs. (9) and (10). The full (open) circles correspond to the regime of full (partial) l mixing for a field of -877 mV/cm. The horizontal dashed line indicates the core-fluorescence rate used as internal clock. The thick solid lines in (a) and (b) correspond to the predictions of our kinetic model assuming full l mixing and n^{-4} scaling of the autoionization rate $k_{\rm a}$ [Eq. (11)].

-877 mV/cm is approximately three times larger than the Inglis-Teller field at $n = 90$ and indeed corresponds to the regime where complete l mixing is expected [25,26]. Fitting the value of $\gamma^{\rm Stark}$ to the experimental data in this range yields a value $\gamma^{\rm Stark} = 8(3) \times 10^{15}$ s^{-1}, where the error bar originates from the uncertainties in the value of the interaction time τ used in our kinetic model (6 ns $< \tau <$ 16 ns). The thick full line in Fig. 4(b) corresponds to the autoionization rates determined with Eq. (11) and starts deviating from the rates extracted from the experimental data below $n = 90$. The deviation, which implies lower autoionization rates than expected from the n^{-4} scaling law, indicates that the experimental signal in this range stems from Stark states with reduced low-l character compared to fully l-mixed Stark states. This behavior is consistent with the observation that the discrete structure observed in the spectra below $n = 80$ corresponds to a purely hydrogenic Rydberg series with zero quantum defect (see also discussion in Refs. [41–44]).

The value of $\gamma^{\rm Stark}$ determined from our experiment is extremely large and implies autoionization rates in the low- or even sub-femtosecond range for the lowest values of n and

l, comparable with Auger decay rates [45]. Measurements of core-excited Rydberg states in other alkaline-earth-metal atoms have also revealed very fast autoionization (see, e.g., Refs. [8,46,47]). From separate experimental and theoretical studies of the Rydberg series converging to the upper spin-orbit component ($3p_{3/2}$) of the first excited state of Mg^+, we conclude that the fastest autoionization process is the spin-orbit autoionization of the $3p_{3/2}nd_{3/2}$ ($J = 3$) Rydberg series [48], which leads to autoionization rates given by $(1.9 \times 10^{16}/n^{*3})\ s^{-1}$.

The times during which the correlated motion of the two excited electrons can be observed experimentally is restricted by the autoionization rate or the core-fluorescence rate, whichever is faster. Our data indicate that under conditions of complete l mixing by dc-electric fields, the core fluorescence is the dominant process for $n > 80$. Such states thus exist for ~3.8 ns, which is longer than the $[2Rc/n^3]^{-1}$ radial oscillation period at $n = 80$ (78 ps) but shorter than the timescale associated with the inverse state density of Stark states at the Inglis-Teller limit $[2Rc/n^4]^{-1}$ (6.2 ns at $n = 80$). For the nd Rydberg series converging to the Mg^+ $3p_{3/2}$ threshold, the core fluorescence becomes dominant for $n > 350$.

Whereas a large body of experimental and theoretical data is available on core-excited states of the alkaline-earth-metal atoms (see Refs. [49–54] for Mg), few data are available in the literature on their autoionization lifetimes in core-excited, zero-field $n'p_{3/2}nl$ Rydberg states and $n'p_{3/2}nk$ Rydberg Stark states lying *above* the respective $n'p_{1/2}$ ionization thresholds ($n' = 2$–6 for atomic species from Be to Ba). In order to assess the validity of the scaled rate extracted from the experimental spectra, we undertook a theoretical calculation of the energies and widths of the doubly excited $3p_{3/2}nl$ states with $l = 0$–6 [48]. Briefly, the calculation is based on a two-active-electron, configuration-interaction description of the Mg atom, similar to that used for high-lying, doubly excited states of the helium atom [55], combined with the exterior complex-scaling method [56]. A similar approach was used by Fields *et al.* to calculate the energies and autoionization rates of the core-excited $5p_{1/2}np$ and $5p_{1/2}nf$ Rydberg states of Sr [8]. The two valence electrons of the Mg atom are assumed to evolve in an effective, l-dependent potential $V_l(r)$ that describes the effect of the $Mg^{2+}(1s^2 2s^2 2p^6)$ closed-shell core [57], and their mutual Coulomb interaction is treated exactly. The two-electron wave functions are expanded in terms of two-electron, antisymmetrized basis vectors built from one-electron orbitals of the Mg^+ ion. The jj coupling scheme is used because it is the most appropriate for high-n, autoionizing Rydberg states [36]. One-electron radial wave functions are calculated from the potential $V_l(r)$ using a finite-element, Legendre discrete-variable-representation technique [58]. In order to determine the autoionization width, we use the exterior complex-scaling method, following which the radial coordinates r_1 and r_2 of both electrons are rotated into the complex plane by a phase $e^{i\theta}$ beyond a certain radius r_0 [56,58], set to $100\,a_0$ in the present calculation. Diagonalization of the complex-rotated, two-electron Hamiltonian yields a set of complex eigenvalues, the real and imaginary parts of which correspond to their energies and widths, respectively. Convergence is reached when the eigenvalues corresponding to the autoionizing states become independent of the rotation angle θ and of the size of the basis set.

A direct calculation of the autoionization widths of the core-excited, high-n Rydberg Stark states of Mg could not be carried out because the required basis would be far too large. However, they can be estimated from those of the zero-field, unperturbed states following the procedure used by Jones and Gallagher [47]. In jj coupling, a $3p_{3/2}nk$ Stark state can be expressed as a linear combination of $(3p_{3/2}nl_j)_J$ zero-field states, where J is the total angular momentum quantum number, with further admixture of states from other n manifolds above the Inglis-Teller limit. Assuming that Stark mixing is uniform, i.e., that all zero-field states contribute equally, the autoionization rate of a given Stark state can be written, in first approximation, as

$$k_{a,n} \simeq \frac{\sum_{ljJ} k_{a,nljJ}}{8(n-1)} \simeq \frac{\sum_{ljJ} \gamma_{ljJ}}{8n^4}. \tag{12}$$

The number of states with different quantum numbers l, j and J for a given value of n is $8(n-1)$, which can be approximated by $8n$ for large n values. Equation (12) relies on the $k_{a,nljJ} = \gamma_{ljJ} n^{*-3}$ scaling law of the zero-field autoionizing Rydberg states.

Since the autoionization rate drops very rapidly with the orbital angular momentum quantum number l, only those rates that correspond to low l values, and therefore to low J values, play a role in the above sum. Our calculation confirms that states with $J \geqslant 5$ have a rate that can be neglected in first approximation when carrying out the sum in Eq. (12), so that

$$\gamma^{\text{Stark}} \simeq \frac{1}{8} \sum_{J=0}^{4} \sum_{lj} \gamma_{ljJ}. \tag{13}$$

The scaled rates for each individual $(3p_{3/2}nd_j)_J$ series are obtained from the rates calculated for effective principal quantum numbers around $n = 60$. We verified that the calculated rates follow the n^{*-3} scaling law from the $3p_{1/2}$ threshold ($n \simeq 35$ for the $3p_{3/2}$ series) up to $n \simeq 90$, corresponding to the highest Rydberg states included in the calculation. We can therefore directly obtain the theoretical scaled rate for the autoionization of Stark states in the uniform mixing regime from Eq. (13),

$$\gamma_{\text{th}}^{\text{Stark}} = 7.2 \times 10^{15}\ s^{-1}. \tag{14}$$

This value is in agreement, within error bars, with the value of $8(3) \times 10^{15}\ s^{-1}$ derived from the experimental data. Considering the simplicity of the assumptions used to determine the experimental value of γ^{Stark}, along with those used to compute the theoretical estimate from the zero-field rates, we consider the agreement as very satisfactory. The rates determined for the $6p_{1/2}nk$ core-excited Rydberg-Stark states of barium by Jones and Gallagher using an equation similar to Eq. (13), but disregarding j and J, are about a factor of 2 larger than those determined from the measured autoionization widths [47]. Our calculations show that j- and J-dependent couplings are important to describe the autoionization of magnesium Rydberg-Stark states above the $3p_{1/2}$ ionization threshold.

V. CONCLUSION

In this article we have reported on measurements of the decay of core-excited Rydberg states of Mg and have analyzed the competition between autoionization and core fluorescence and its dependence on weak electric fields. In high Rydberg states, the fluorescence of the ion core is not significantly affected by the Rydberg electron and can be used as an internal clock for the determination of autoionization rates. We have extracted scaling laws which describe autoionization rates of the optically accessible $3p_{3/2}nd_{3/2}$ ($J = 3$) Rydberg series [$k_{a,nd} = (1.9 \times 10^{16}/n^{*3})$ s^{-1}] and of fully l-mixed Stark states [$k_{a,\mathrm{Stark}} = (8(3) \times 10^{15}/n^4)$ s^{-1}]. These rates are extremely large and comparable to Auger decay rates at low n values. These rates also imply that the core fluorescence becomes the dominant decay process, and that consequently autoionization becomes negligible, at n values beyond 350 and 80 for $3p_{3/2}nd_{3/2}$ ($J = 3$) Rydberg states and l-mixed Stark states, respectively. These n values can also be interpreted as those for which the core transition becomes equivalent to the transition of the bare ion and the Rydberg electron can be regarded as a spectator.

The results also demonstrate that even the fastest autoionization processes become slow on the (ns) timescale of radiative processes in the ion core at sufficiently high n values. The core fluorescence effectively turns off the autoionization and stabilizes the Rydberg electron for much longer times, extending to the millisecond timescale at n values beyond 100. This mechanism is identical to that enabling the recording of pulsed-field ionization zero-kinetic-energy photoelectron spectra of electronically excited atomic [59] and molecular [60–62] states.

ACKNOWLEDGMENTS

We thank J. A. Agner and H. Schmutz for their contribution to the development of the spectrometer used in this study. This work is supported financially by the Swiss National Science Foundation (Grant No. 200020-172620) and the European Research Council through an advanced grant under the European Union's Horizon 2020 research and innovation programme (Grant No. 743121).

[1] J. Berkowitz, *Photoabsorption, Photoionization and Photoelectron Spectroscopy* (Academic, New York, 1979).
[2] I. C. Percival, Proc. R. Soc. London A **353**, 289 (1977).
[3] J. G. Leopold, I. C. Percival, and A. S. Tworkowski, J. Phys. B: At. Mol. Phys. **13**, 1025 (1980).
[4] U. Eichmann, P. Brockmann, V. Lange, and W. Sandner, J. Phys. B: At. Mol. Opt. Phys. **22**, L361 (1989).
[5] U. Eichmann, V. Lange, and W. Sandner, Phys. Rev. Lett. **64**, 274 (1990).
[6] U. Eichmann, V. Lange, and W. Sandner, Phys. Rev. Lett. **68**, 21 (1992).
[7] G. Tanner, K. Richter, and J.-M. Rost, Rev. Mod. Phys. **72**, 497 (2000).
[8] G. Fields, X. Zhang, F. B. Dunning, S. Yoshida, and J. Burgdörfer, Phys. Rev. A **97**, 013429 (2018).
[9] H. A. Griem, *Spectral Line Broadening by Plasmas*, Pure and Applied Physics (Academic, New York, 1974).
[10] V. L. Jacobs, J. Davis, and P. C. Kepple, Phys. Rev. Lett. **37**, 1390 (1976).
[11] D. A. Harmin, Phys. Rev. Lett. **57**, 1570 (1986).
[12] D. C. Griffin, M. S. Pindzola, and C. Bottcher, Phys. Rev. A **33**, 3124 (1986).
[13] C. Bottcher, D. C. Griffin, and M. S. Pindzola, Phys. Rev. A **34**, 860 (1986).
[14] K. LaGattuta, I. Nasser, and Y. Hahn, Phys. Rev. A **33**, 2782 (1986).
[15] K. LaGattuta, I. Nasser, and Y. Hahn, J. Phys. B: At. Mol. Phys. **20**, 1565 (1987).
[16] K. LaGattuta, I. Nasser, and Y. Hahn, J. Phys. B: At. Mol. Phys. **20**, 1577 (1987).
[17] D. S. Belić, G. H. Dunn, T. J. Morgan, D. W. Mueller, and C. Timmer, Phys. Rev. Lett. **50**, 339 (1983).
[18] A. Müller, D. S. Belić, B. D. DePaola, N. Djurić, G. H. Dunn, D. W. Mueller, and C. Timmer, Phys. Rev. Lett. **56**, 127 (1986).
[19] A. Müller, D. S. Belić, B. D. DePaola, N. Djurić, G. H. Dunn, D. W. Mueller, and C. Timmer, Phys. Rev. A **36**, 599 (1987).
[20] J. G. Story, L. D. Van Woerkom, and W. E. Cooke, Phys. Rev. A **34**, 4508(R) (1986).
[21] J. G. Story, B. J. Lyons, and T. F. Gallagher, Phys. Rev. A **51**, 2156 (1995).
[22] L. Ko, V. Klimenko, and T. F. Gallagher, Phys. Rev. A **59**, 2126 (1999).
[23] J. Nunkaew and T. F. Gallagher, Phys. Rev. A **81**, 023417 (2010).
[24] J. Dubau and S. Volonté, Rep. Prog. Phys. **43**, 199 (1980).
[25] W. A. Chupka, J. Chem. Phys. **98**, 4520 (1993).
[26] T. F. Gallagher, *Rydberg Atoms* (Cambridge University, Cambridge, England, 1994).
[27] F. Merkt, S. Willitsch, and U. Hollenstein, in *Handbook of High-Resolution Spectroscopy*, Vol. 3, edited by M. Quack and F. Merkt (Wiley, New York, 2011), pp. 1617–1654.
[28] R. Mukherjee, J. Millen, R. Nath, M. P. A. Jones, and T. Pohl, J. Phys. B: At. Mol. Opt. Phys. **44**, 184010 (2011).
[29] F. B. Dunning, T. C. Killian, S. Yoshida, and J. Burgdörfer, J. Phys. B: At. Mol. Opt. Phys. **49**, 112003 (2016).
[30] K.-L. Pham, H. Lehec, W. Maineult, S. Lepoutre, P. Pillet, T. F. Gallagher, and P. Cheinet, in *Proceedings of the 13th European Conference on Atoms, Molecules and Photons, April 2019* (unpublished).
[31] P. McQuillen, X. Zhang, T. Strickler, F. B. Dunning, and T. C. Killian, Phys. Rev. A **87**, 013407 (2013).
[32] G. Lochead, D. Boddy, D. P. Sadler, C. S. Adams, and M. P. A. Jones, Phys. Rev. A **87**, 053409 (2013).
[33] H. Lehec, A. Zuliani, W. Maineult, E. Luc-Koenig, P. Pillet, P. Cheinet, F. Niyaz, and T. F. Gallagher, Phys. Rev. A **98**, 062506 (2018).
[34] W. E. Cooke, T. F. Gallagher, S. A. Edelstein, and R. M. Hill, Phys. Rev. Lett. **40**, 178 (1978).

[35] W. E. Cooke, in *Atomic Physics 7*, edited by D. Kleppner and F. Pipkin (Springer, Boston, 1981), pp. 167–180.
[36] M. Aymar, C. H. Greene, and E. Luc-Koenig, Rev. Mod. Phys. **68**, 1015 (1996).
[37] L. Pruvost, P. Camus, J.-M. Lecomte, C. R. Mahon, and P. Pillet, J. Phys. B: At. Mol. Opt. Phys. **24**, 4723 (1991).
[38] H. Lehec, Ph.D. thesis, Université de Paris Saclay, 2017.
[39] M. Génévriez, D. Wehrli, J. A. Agner, and F. Merkt, Int. J. Mass Spectrom. **435**, 209 (2019).
[40] A. Kramida, Yu. Ralchenko, J. Reader, and NIST ASD Team, NIST Atomic Spectra Database (ver. 5.6.1), Available: `https://physics.nist.gov/asd` [2019, January 29] (National Institute of Standards and Technology, Gaithersburg, MD, 2018).
[41] F. Remacle, R. D. Levine, E. W. Schlag, H. L. Selzle, and A. Held, J. Phys. Chem. **100**, 15320 (1996).
[42] F. Remacle, U. Even, and R. D. Levine, J. Phys. Chem. **100**, 19735 (1996).
[43] M. Bixon and J. Jortner, J. Chem. Phys. **103**, 4431 (1995).
[44] P. Bellomo, D. Farrelly, and T. Uzer, J. Chem. Phys. **107**, 2499 (1997).
[45] C. Miron and P. Morin, in *Handbook of High-Resolution Spectroscopy*, Vol. 3, edited by M. Quack and F. Merkt (Wiley, New York, 2011), pp. 1655–1689.
[46] E. Y. Xu, Y. Zhu, O. C. Mullins, and T. F. Gallagher, Phys. Rev. A **33**, 2401 (1986).
[47] R. R. Jones and T. F. Gallagher, Phys. Rev. A **39**, 4583 (1989).
[48] M. Génévriez, D. Wehrli, and F. Merkt (unpublished).
[49] C. J. Dai, G. W. Schinn, and T. F. Gallagher, Phys. Rev. A **42**, 223 (1990).
[50] G. W. Schinn, C. J. Dai, and T. F. Gallagher, Phys. Rev. A **43**, 2316 (1991).
[51] M. D. Lindsay, L.-T. Cai, G. W. Schinn, C.-J. Dai, and T. F. Gallagher, Phys. Rev. A **45**, 231 (1992).
[52] M. D. Lindsay, C.-J. Dai, L.-T. Cai, T. F. Gallagher, F. Robichaux, and C. H. Greene, Phys. Rev. A **46**, 3789 (1992).
[53] M. D. Lindsay, C. J. Dai, B. J. Lyons, C. R. Mahon, and T. F. Gallagher, Phys. Rev. A **50**, 5058 (1994).
[54] B. J. Lyons, J. A. Shanchuck, J. Hostetler, and T. F. Gallagher, Phys. Rev. A **52**, 4586 (1995).
[55] G. Lagmago Kamta, B. Piraux, and A. Scrinzi, Phys. Rev. A **63**, 040502(R) (2001).
[56] B. Simon, Phys. Lett. A **71**, 211 (1979).
[57] E. Luc-Koenig, A. Lyras, J.-M. Lecomte, and M. Aymar, J. Phys. B: At. Mol. Opt. Phys. **30**, 5213 (1997).
[58] T. N. Rescigno and C. W. McCurdy, Phys. Rev. A **62**, 032706 (2000).
[59] F. Merkt, J. Chem. Phys. **100**, 2623 (1994).
[60] W. Kong, D. Rodgers, and J. W. Hepburn, Chem. Phys. Lett. **221**, 301 (1994).
[61] H. Palm and F. Merkt, Chem. Phys. Lett. **284**, 419 (1998).
[62] H. Palm and F. Merkt, Phys. Rev. Lett. **81**, 1385 (1998).